Adaptive transmission in heterogeneous networks

Zhao Li[1] ✉, Lu Zhen[1], Xiaoqin Dai[1], Biao Shen[1], Yujiao Bai[1], Xiaohui Ren[1], Kang G. Shin[2]

[1]*State Key Laboratory of Integrated Service Networks, Xidian University, No. 2 South Taibai Road, Xian, People's Republic of China*
[2]*Department of Electrical Engineering and Computer Science, The University of Michigan, 2260 Hayward Street, Ann Arbor, USA*
✉ *E-mail: zli@xidian.edu.cn*

Abstract: An **A**daptive tran**S**mission mechanism exploiting both interference lo**C**ality and the relationship between d**E**sired sig**N**al and in**T**erference (**ASCENT**) is proposed for uplink transmission in heterogeneous networks. The authors adopt both X channel and Z channel models according to which spatial signal processing is designed. In the X channel, the picocell base station (PBS) exploits information the macrocell base station (MBS) shares to cancel local interference, and cooperatively decodes the data carried by strong interference from a macro-user (MU), which is then fed to the MBS. As a result, a pico-user (PU) can transmit simultaneously with an MU on the same channel. In addition, adaptive reception is employed to achieve good tradeoff between interference suppression and the desired level of signal distortion. For the Z channel, the PU and the PBS adopt signal processing suitable for their own channel state. At a PBS, interference cancellation is adopted to eliminate disturbance from an MU via inter-base station collaboration. ASCENT is also extended to the case of multiple picocells. The authors' simulation results show that in X channel mode, the achievable uplink rate of an MU can be significantly enhanced. In the case of Z channel, the PU's rate is improved while guaranteeing the MU's data rate.

1 Introduction

With the advance of communication technology, the demand for high data transmission rates is increasing rapidly, imposing difficulties on existing cellular systems. Leveraging the increased spatial reuse from smaller cells is a promising direction [1]. By deploying low-power and small-coverage base stations (BSs) in the original cellular systems, users' data rate could be improved. In addition, small BSs deployed in a dense subscriber area can greatly enhance the system capacity [2]. This heterogeneous network (HetNet) has received significant attention for 3rd generation partnership project (3GPP) and been adopted as a standard technique in Long-term evolution advanced (LTE-A) [3].

Due to the scarcity and cost of spectral spectrum, it is impractical to allocate extra frequency bands for small cells. Consequently, when various types of cells (i.e. macro, pico and femtocells) share the same band, their mutual interference becomes a critical issue, restricting communication performance. The interferences in HetNet can be attributed to four sources: unplanned deployments, closed subscriber group (CSG) access, power difference between nodes and range expanded users [4]. Some works on interference management (IM) in small cell networks [5, 6] employed interference avoidance in the time or the frequency domain by allocating orthogonal channels to small interfering cells. Then, by employing beamforming (BF) or directional antennas for spatial reuse in a multi-cell setup, such waste of spectral resources can be avoided [7]. Soft frequency reuse was proposed in [8], which can be applied to HetNet to suppress inter-cell interferences (ICIs). Furthermore, in order to solve the interference problem in HetNet, 3GPP proposes enhanced ICI coordination by introducing almost blank subframes in time domain [9].

Interference alignment (IA) [10], a novel interference control mechanism that can be applied to HetNet, has received significant attention. With IA, interferences are confined to a subspace orthogonal to the expected signal space, so that desired signal and interference can be separated from each other. In [11], a linear transceiver based on IA for multi-input multi-output (MIMO) HetNet is proposed. With the method, ICI from pico-BSs to

macro-users (MUs) is properly aligned and both ICI and inter-user interference (IUI) are nullified. The authors of [12] proposed a hierarchical IA scheme by applying IA to a HetNet environment to mitigate both the inter-tier interference between a macrocell and picocells, and the IUI between MUs. Two different picocell access modes: open subscriber group and CSG, are considered. The use of IA is shown to be able to reduce consumption of degrees of freedom (DoFs) for interference elimination at receiver nodes and achieve higher throughput than the case without IA.

However, the feasibility of IA is highly dependent on the system parameter settings [13–15], such as the number of transmitters and receivers, the number of transmit and receive antennas and so on. Hence, in some cases IA cannot enable multiple interference-free concurrent transmissions. As a result, researchers exploit cooperative capability at either transmitter or receiver side, and design mechanisms by combining IA with other IM methods [16, 17]. A scheme based on interference alignment and cancellation (IAC) was proposed in [16] for multi-hop mesh networks. By introducing a helper node, multiple concurrent packet transmissions can be achieved using fewer time slots. The authors of [17] designed an interference alignment and neutralisation based coordinated multi-point transmission scheme for cellular networks. Both interference neutralisation and IA are employed for appropriately adjusting interfering signals carrying identical and different information, so that concurrent transmissions of multiple data streams can be supported.

However, the above existing works do not take sufficient practical factors into account, hence limiting their applicability. On the one hand, some useful properties such as *interference locality* [18] and *partial connectivity* [19–23] are not exploited, thus hindering the effective improvement of communication performance. On the other hand, some ideal or specific model based methods may not be applicable to practical system, incurring conclusions therein become invalid. As for the latter case, even though some schemes may be applicable with minor modifications, performance degradation is likely to occur. To remedy this deficiency, the authors in [19–22] take large-scale fading and/or transmit power difference between different types of nodes into account to design

IA schemes in partially connected networks where the unperceived interfering links are disconnected. In [19], the feasibility of IA in partially connected networks was studied, whereas in [20] derived a closed-form solution to implement IAC. Both works of [19, 20] focus on the uplink design. Multiple IA mechanisms for partially connected downlink networks were proposed in [21–23] where the decision of whether an interfering link exists is based on a pre-defined threshold according to either the distance from an interferer to its victim receiver or the signal to interference ratio at a receiver. However, how to adaptively select proper threshold adapting to various network deployments and dynamic channel conditions has not been well addressed. In addition, since the aforementioned signal processing methods inevitably cause the desired signal power loss (i.e. cost) while suppressing or mitigating interferences (i.e. benefit), not only the unperceivable interfering links [23] but also those perceived ones whose processing cost outweigh their benefits should be discarded. Thus a practical model that can be used to determine whether interference should be processed so as to achieve a flexible tradeoff between the cost and benefit in a dynamically changing network environment is in great demand. Moreover, in practical use the various network topologies will affect the interference situation. The adaptability of transmission and reception schemes to this variation is a key factor for realising both high system performance and low processing complexity.

In this paper, we focus on the uplink transmission in HetNet consisting of spatially overlapped macrocell and picocells that share the same frequency band. By considering the aforementioned practical factors, we propose an adaptive uplink transmission mechanism in HetNet that exploits both interference locality and the relationship between the desired signal and interference (**A**daptive tran**S**mission mechanism exploiting both interference lo**C**ality and the relationship between d**E**sired sig**N**al and in**T**erference – ASCENT). Here we name the fading effect on interfering signal as *interference locality* [18]. By employing IA and cancellation as well as reception scheme adaptation, concurrent data transmissions of macro and picocell users are achieved.

This paper makes the following main contributions:

• Introduction of a criterion in terms of the rate performance loss tolerance w.r.t. an MU, which is used for adaptive consideration of uplink interference from a pico-user (PU) to the macrocell BS (MBS) and can adapt to various network deployments and dynamic channel conditions. This criterion generalises the concept of partial connectivity since a perceived interference can also be discarded for the benefit of the overall system design.
• Derivation of an adaptive reception mode selection criterion based on the spatial correlation and strength of desired signal and interference, according to which a good tradeoff between interference suppression and desired level of signal distortion is achieved.
• On the basis of the above two criteria, an adaptive transmission mechanism with joint processing at both the transmitter and receiver sides is developed for the uplink communication of HetNet consisting of macrocell and picocell. By exploiting BS-side cooperation, cross-tier interference is properly managed, thus realising multiple concurrent data transmissions of macrocell and picocell users.

The remaining of this paper is organised as follows. Section 2 describes the system model, while Sections 3 and 4 present the adaptive transmission scheme and its extended version, respectively. Section 5 evaluates the proposed algorithm. Finally, Section 6 concludes the paper.

Throughout this paper, we use the following notation. The set of complex numbers is denoted as $\mathbb{C}$, while vectors and matrices are represented by bold lower-case and upper-case letters, respectively. The Hermitian (or conjugate transpose), transpose and inverse of a vector or a matrix are denoted as $(\cdot)^{\mathrm{H}}$, $(\cdot)^{\mathrm{T}}$ and $(\cdot)^{-1}$, respectively. $\mathbb{E}(\cdot)$ represents the statistical expectation and $\|\cdot\|$ represents the Euclidean norm.
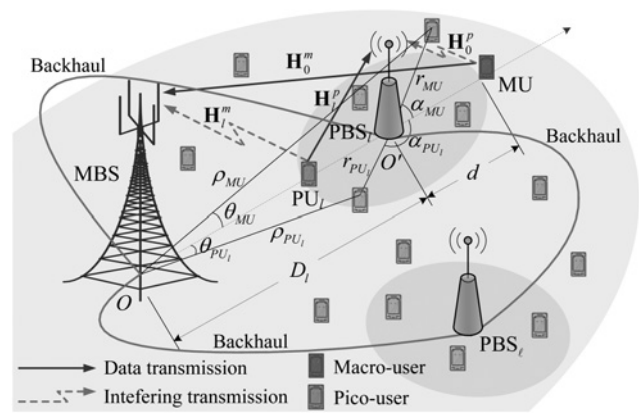

Fig. 1 *System model*

2 System model

Consider uplink communication in a HetNet consisting of one MBS, L picocell BSs (PBSs), randomly distributed MUs and PUs. Picocells share the same spectrum band with the macrocell. Since PBSs are usually operator-installed infrastructures [4], thus inter-picocell interference can be properly managed. As a consequence, in this paper, we only focus on the cross-tier interference issue in HetNet. For simplicity, we assume all picocells show the same statistical characteristics. For clarity of presentation, only one active picocell indexed by $l \in \{1, \ldots, L\}$ in which one PU_l is scheduled to perform uplink transmission, is taken into account as shown in Fig. 1. Without ambiguity, the subscript l is omitted for simplicity in the following discussion.

As Fig. 1 shows, the distance between MBS and PBS is D, and the picocell operates in an open mode and allows all users to access. The radio range of a picocell, denoted by d, is 300 m or less [4]. Although a PBS can support only a small number of users – usually a few tens of users [4] due to its capacity limit – we assume that the picocell is lightly loaded and can thus admit users' access requests within its range. As for users within the overlapping area of macrocell and picocell, they can select a proper access point or BS by comparing downlink reference signals received from candidate BSs. In this way, the radius of the picocell d should decrease as D decreases. Otherwise, when PBS is too close to MBS, although a user is within the coverage of PBS, the received signal from MBS may be much stronger than that from PBS due to the transmit power difference between MBS and PBS, resulting in an inappropriate selection of MBS as the access point. Therefore, a threshold-based mechanism could be adopted in conjunction with the above scheme, with which the strength of downlink signal is compared to a preset threshold to determine which BS to access. The threshold can be determined based on the average strength of received signal from PBS at distance d. For example, if the received reference signal power from PBS exceeds the threshold, the mobile user accesses PBS even if a stronger signal from MBS is received. Otherwise, the mobile user selects the one from which a stronger downlink signal is received. With this BS selection strategy, PUs can still access the PBS as long as the received reference signal power from PBS exceeds the threshold even when the distance between MBS and PBS is not far enough. When the distance from MU to PBS is smaller than d, an MU accesses PBS and becomes a PU with high probability since the path loss is more dominant than small-scale fading, whereas the PU accesses MBS with high probability when the distance from the PU to PBS is greater than d.

Note that the deployment of small cells aims to offload the macrocell and boost spectral efficiency via spatial reuse [4]. Thus, we set the range of D large enough, and assume d is fixed for simplicity. Then, a simplified BS-selection strategy is adopted, with which users within the range of the picocell will access PBS; otherwise, they will choose MBS.

Although there are multiple mobile users in the HetNet, we assume that the transmission resource is divided into time slots and multiple frequency bands. Both macrocell and picocell operate in a synchronised slot structure. In each time slot, BS allocates different resource block (RB), i.e. a time-and-frequency resource, to its users, so that co-channel interference (CCI) within a cell is avoided. Thus, for an arbitrary RB, only one user is scheduled in each macrocell and picocell, respectively, for the uplink transmission [24]. As a result, a simplified system model is obtained.

As Fig. 1 shows, the distance from MU and PU to MBS can be calculated as

$$\rho_{\text{MU}} = (D + r_{\text{MU}} \cos \alpha_{\text{MU}})/\cos \theta_{\text{MU}} \qquad (1)$$

$$\rho_{\text{PU}} = (D + r_{\text{PU}} \cos \alpha_{\text{PU}})/\cos \theta_{\text{PU}}. \qquad (2)$$

For simplicity, the height of BS is ignored in the analysis. Let r_{MU} and r_{PU} denote the distance from MU and PU to PBS, respectively.

The randomness of mobile users' geographical position makes the analysis difficult. However, one can easily see that as $r_{\text{MU}} = d + \varepsilon$, where ε is a positive number and ε approaches 0, the interference from MU to PBS is the strongest. On the other hand, as $r_{\text{PU}} = d - \varepsilon$, the desired signal from PU to PBS is the weakest. Moreover, if the MBS is the target receiver, $\alpha_{\text{MU}} = 0$ renders a weak desired signal from MU to MBS, whereas $\alpha_{\text{PU}} = \pi$ yields strong interference from PU to MBS. Consequently, the network topology in which MBS, PU, PBS, MU are successively and linearly deployed shows the worst case for the uplink transmission of both MU and PU, since the signal-to-interference-plus-noise ratio (SINR) at MBS and PBS is significantly deteriorated.

Let N_r^{p}, N_r^{m}, N_t^{p} and N_t^{m} be the number of antennas at PBS, MBS, PU and MU. Channel matrices from MU to MBS and PBS are denoted by $\boldsymbol{H}_0^{\text{m}} \in \mathbb{C}^{N_r^{\text{m}} \times N_t^{\text{m}}}$ and $\boldsymbol{H}_0^{\text{p}} \in \mathbb{C}^{N_r^{\text{p}} \times N_t^{\text{m}}}$, whereas from PU to PBS and MBS are expressed as $\boldsymbol{H}_1^{\text{p}} \in \mathbb{C}^{N_r^{\text{p}} \times N_t^{\text{p}}}$ and $\boldsymbol{H}_1^{\text{m}} \in \mathbb{C}^{N_r^{\text{m}} \times N_t^{\text{p}}}$, respectively. A spatially uncorrelated Rayleigh flat fading channel model is assumed so as to model the elements of the above matrices as independent and identically distributed zero-mean unit-variance complex Gaussian random variables. We assume that all users experience block fading. Since PBS and MBS could be deployed by the same operator, they can be scheduled so that their transmissions of training sequence are serialised (to avoid collision). Each user can accurately estimate channel state information (CSI) based on the received training signal from its associated (i.e. serving) BS and unassociated BS (i.e. victim in the uplink case), respectively, and feed it back to its associated BS via a low-rate error-free link. CSI can be shared between BSs via reliable backhaul so that $\boldsymbol{H}_0^{\text{m}}$ and $\boldsymbol{H}_1^{\text{m}}$ are available at PBS for its signal processing. Since our focus is on the cross-tier interference between multiple uplink transmissions, a user needs to estimate at most two CSIs corresponding to the data channel and interfering channel, respectively, thus minor modification is required as compared with those conventional mechanisms where only one CSI w.r.t. the desired data transmission is estimated. As for the BSs, no modification is required. Based on the above description, the CSI-related burden of our scheme does not increase with the scale of network. Besides, in our mechanism, the backhaul is also used for necessary data sharing amongst multiple BSs. We assume the delay of the links dedicated to CSI and signalling delivery is negligible relative to the time scale on which the channel state varies. MU employs spatial multiplexing to make full use of its spatial resource. The transmit power is equally distributed over multiple spatial sub-channels. Since the picocell is deployed as an auxiliary to improve the capacity and coverage of existing cellular systems, we consider in this paper that the picocell has subordinate features compared with the macrocell, and BF is adopted at PU. For simplicity, in the following discussion we let $N_r^{\text{p}} = N_r^{\text{m}} = N_t^{\text{p}} = N_t^{\text{m}} = 2$.

Note that although only one picocell is considered for simplicity, the proposed mechanism can be applied to the more general case

where multiple picocells, say L, are deployed within the coverage of macrocell. Details can be found in Section 4.

3 Adaptive transmission exploiting interference locality and signal-interference interrelation

We now detail the adaptive transmission scheme exploiting interference locality and the relationship between desired signal and interference (ASCENT). First, we describe basic signal processing and analyse interference locality. Due to the variation of network deployment and channel conditions, interference situation cannot remain unchanged, two interference models are provided according to the criterion used for adaptive consideration of uplink interference from PU to MBS: (i) the X channel model [25] in which all cross-tier interferences are taken into account; and (ii) the Z channel model where the weak interference is ignored. Then, in each of these models, signal processing for uplink transmission is designed.

3.1 Basic signal processing and interference locality analysis

Assume that the picocell operates in open mode and is lightly-loaded. Mobile user selects the access point following the simplified strategy given in Section 2. Since the uplink transmissions of MU and PU share the same spectrum band, there will be interference at MBS and PBS.

PU employs BF and sends x_1 to PBS, whereas MU adopts SM and sends x_{01} and x_{02} simultaneously to MBS. $\mathbb{E}(\|x_1\|^2) = \mathbb{E}(\|x_{0i}\|^2) = 1$ where $i = 1, 2$, holds. The transmit power of MU, denoted by P_{m}, is equally distributed over two data streams. Due to path loss, the received signal at MBS is expressed as
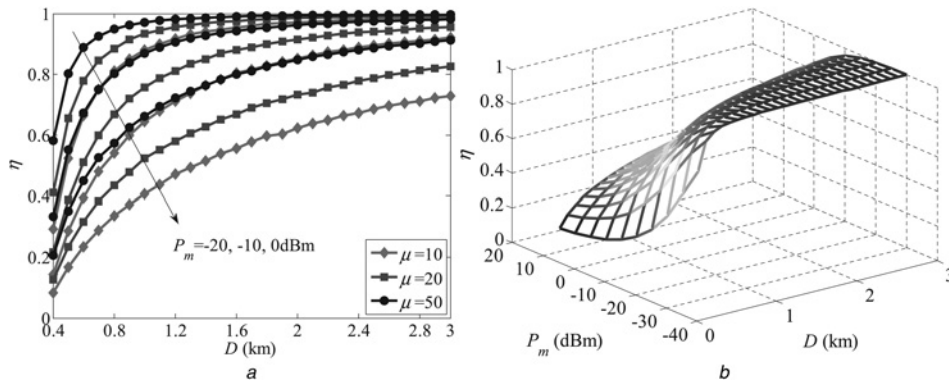
$$\boldsymbol{y}_{\text{m}} = \sqrt{\frac{P_{\text{m}}}{2}} \rho_{\text{MU}}^{-\alpha/2} \boldsymbol{H}_0^{\text{m}} \boldsymbol{P}_0 \boldsymbol{x}_0 + \sqrt{P_{\text{p}}} \rho_{\text{PU}}^{-\alpha/2} \boldsymbol{H}_1^{\text{m}} \boldsymbol{p}_1 x_1 + \boldsymbol{n} \qquad (3)$$

where $\boldsymbol{P}_0 = [\boldsymbol{p}_{01} \quad \boldsymbol{p}_{02}]$ and $\boldsymbol{x}_0 = [x_{01} \quad x_{02}]^{\text{T}}$. Column vectors $\boldsymbol{p}_{01}$, $\boldsymbol{p}_{02}$ and $\boldsymbol{p}_1$ are the precoders for data symbols x_{01}, x_{02} and x_1, respectively. P_{p} denotes the transmit power of PU. $\boldsymbol{n}$ is the additive white Gaussian noise vector whose elements have zero-mean and variance σ_{n}^2. For simplicity, the path loss from MU and PU to MBS are modelled as $\rho_{\text{MU}}^{-\alpha/2}$ and $\rho_{\text{PU}}^{-\alpha/2}$, respectively, where α represents for the path loss factor and we set $\alpha = 2$ as in [26]. One can also adopt the more accurate path loss model as given in [27] and take into account the antenna gain at MBS and PBS [28], similar results can be achieved. Due to space limitation, we do not elaborate this any further in this paper.

Applying the singular value decomposition to $\boldsymbol{H}_0^{\text{m}}$ and $\boldsymbol{H}_1^{\text{p}}$, we get $\boldsymbol{H}_0^{\text{m}} = \boldsymbol{U}_0^{\text{m}} \boldsymbol{\Lambda}_0^{\text{m}} (\boldsymbol{V}_0^{\text{m}})^{\text{H}}$ and $\boldsymbol{H}_1^{\text{p}} = \boldsymbol{U}_1^{\text{p}} \boldsymbol{\Lambda}_1^{\text{p}} (\boldsymbol{V}_1^{\text{p}})^{\text{H}}$ where

$$\boldsymbol{U}_0^{\text{m}} = [\boldsymbol{u}_{01}^{\text{m}} \quad \boldsymbol{u}_{02}^{\text{m}}], \quad \boldsymbol{\Lambda}_0^{\text{m}} = \begin{bmatrix} \lambda_{01}^{\text{m}} & 0 \\ 0 & \lambda_{02}^{\text{m}} \end{bmatrix}, \quad \boldsymbol{V}_0^{\text{m}} = [\boldsymbol{v}_{01}^{\text{m}} \quad \boldsymbol{v}_{02}^{\text{m}}],$$

$$\boldsymbol{U}_1^{\text{p}} = [\boldsymbol{u}_{11}^{\text{p}} \quad \boldsymbol{u}_{12}^{\text{p}}], \quad \boldsymbol{\Lambda}_1^{\text{p}} = \begin{bmatrix} \lambda_{11}^{\text{p}} & 0 \\ 0 & \lambda_{12}^{\text{p}} \end{bmatrix} \quad \text{and} \quad \boldsymbol{V}_1^{\text{p}} = [\boldsymbol{v}_{11}^{\text{p}} \quad \boldsymbol{v}_{12}^{\text{p}}].$$

Due to the auxiliary feature of small cell compared with the macrocell, we give the latter higher priority. MU and MBS employ signal processing suitable for $\boldsymbol{H}_0^{\text{m}}$, i.e. adopt $\boldsymbol{P}_0 = \boldsymbol{V}_0^{\text{m}}$ and $\boldsymbol{F}_0 = \boldsymbol{U}_0^{\text{m}}$ as the precoder and receive filters, respectively, so as to achieve as high transmission rate as possible. If PU operates similarly without considering its interference to MBS, $\boldsymbol{p}_1 = \boldsymbol{v}_{11}^{\text{p}}$ is employed, then the reception at MBS would be deteriorated. Substituting the above parameters into (3), we obtain the estimated signal at MBS as

Fig. 2 *Variation of η with different parameters*

a η against D for different P_m and μ
b η against D and P_m under $\mu = 20$

$$\bar{y}_{\mathrm{m}} = \sqrt{\frac{P_{\mathrm{m}}}{2}} \rho_{\mathrm{MU}}^{-\alpha/2} \begin{bmatrix} \lambda_{01}^{\mathrm{m}} x_{01} \\ \lambda_{02}^{\mathrm{m}} x_{02} \end{bmatrix} + \sqrt{P_{\mathrm{p}}} \rho_{\mathrm{PU}}^{-\alpha/2} (U_0^{\mathrm{m}})^{\mathrm{H}} H_1^{\mathrm{m}} p_1 x_1 + (U_0^{\mathrm{m}})^{\mathrm{H}} n \tag{4}$$

Then, the achievable rate of MU's data x_{0i} ($i = 1, 2$) normalised by bandwidth can be calculated as

$$R_{0i} = \log_2 \left\{ 1 + \frac{(P_{\mathrm{m}}/2)\rho_{\mathrm{MU}}^{-\alpha}(\lambda_{0i}^{\mathrm{m}})^2}{\sigma_{\mathrm{n}}^2 + P_{\mathrm{p}} \rho_{\mathrm{PU}}^{-\alpha} \|(u_{0i}^{\mathrm{m}})^{\mathrm{H}} H_1^{\mathrm{m}} p_1\|^2} \right\} \tag{5}$$

In the fraction of (5), the term $P_{\mathrm{p}} \rho_{\mathrm{PU}}^{-\alpha} \|(u_{0i}^{\mathrm{m}})^{\mathrm{H}} H_1^{\mathrm{m}} p_1\|^2$ indicates the interference to the transmission of x_{0i}. Since the transmit power of MU is much higher than that of PU, the interference caused by MU to PBS should always be taken into account. However, as PU imposes relatively weak interference on MBS, it can be ignored when its impact is small. Then, the uplink rate of MU can be re-calculated by omitting the interference part in the denominator of (5). The newly-computed rate is denoted as $\tilde{R}_{0i}$ ($i = 1, 2$).

On the basis of the geographical topology of HetNet and transmit power difference between nodes, cross-tier interference may be ignored as its impact on the uplink transmission of MU is small enough. Then, the transmission from PU to PBS can be adjusted according to their own channel features; $p_1 = v_{11}^{\mathrm{p}}$ is adopted in this paper. On the other hand, uplink performance of MU will not be obviously affected. To exploit interference locality, we define η as

$$\eta = \frac{R_{01} + R_{02}}{\tilde{R}_{01} + \tilde{R}_{02}} \tag{6}$$

η is the ratio of actual sum-rate $R_{01} + R_{02}$ to approximate sum-rate $\tilde{R}_{01} + \tilde{R}_{02}$. The difference between the above two calculations is whether cross-tier interference from PU to MBS is considered. Actually, $\tilde{R}_{01} + \tilde{R}_{02}$ can also be called ideal sum-rate, i.e. no interference is introduced to MBS. The closer η approaches 1, the less inaccurate the sum-rate computation becomes due to negligence of cross-tier interference.

Provided that the ratio of P_{m} to P_{p} is μ, i.e. $P_{\mathrm{m}} = \mu P_{\mathrm{p}}$, $r_{\mathrm{MU}} = r_{\mathrm{PU}} = d = 300$ m [4], $\alpha_{\mathrm{MU}} = 0$, $\alpha_{\mathrm{PU}} = \pi$, and $\theta_{\mathrm{MU}} = \theta_{\mathrm{PU}} = 0$. The interval of D is chosen [0.4, 3] km. Although μ may vary within a certain range, in this paper, for simplicity we investigate $\mu \in \{10, 20, 50\}$. The same conclusion can be drawn even with different values of μ. Fig. 2 shows the variation of η with different parameters.

Fig. 2a plots the values of η against D for different P_{m} and μ. As shown in the figure, given P_{m} and μ, η grows as D increases. For fixed D and μ, η reduces as P_{m} increases. When both D and P_{m} are fixed, η grows as μ increases. It can be explained as follows. Since the ratio of P_{m} to P_{p}, μ is fixed, when D is small, both desired signal and interference are strong at MBS. Noise is weak

compared with interference, so ignoring interference results in much higher rate than that with interference considered. Thus, high inaccuracy results and a small η is produced. As D increases, both desired signal and interference power get lower at MBS, while the noise remains unchanged. Thus, noise power gradually becomes the dominant factor affecting the achievable rate. Consequently, the performance gap with and without cross-tier interference considered becomes small, yielding η close to 1. Provided with fixed D, since P_{p} changes with P_{m} proportionally, the impact of interference on rate computation becomes more significant as P_{m} increase, thus reducing η. When both D and P_{m} are fixed, since the strength of interference from PU to MBS decreases as μ increases, η grows with an increase of μ. Fig. 2b shows the values of η against P_{m} and D under $\mu = 20$. One can see that η grows as D increases, and decreases as P_{m} increases. The patterns shown in Fig. 2b are consistent with those in Fig. 2a.

On the basis of the above discussion, we define a threshold η_{th} indicating the rate performance loss tolerance w.r.t. MU. Then, the criterion exploiting interference locality can be expressed as: if $\eta \geq \eta_{\mathrm{th}}$, interference from PU to MBS can be ignored; otherwise, it should be considered. The selection of η_{th} will have impact on uplink transmission of MU. If η_{th} is too small, strong interference may be ignored incorrectly, thus resulting in higher MU performance loss.

3.2 Signal processing in X channel model

Here we propose signal processing based on non-ignorable cross-tier interference in which both IA and cancellation are employed. As given by (3), the signal observed by MBS is composed of two desired data streams from MU and one interfering signal from PU. Since MBS has only two antennas, the above-mentioned three signal components cannot be distinguished. We first design precoding schemes at MU and PU, with which x_{01} and x_{02} are transmitted through sub-channels matching H_0^{m}, i.e. $P_0 = V_0^{\mathrm{m}}$ is adopted. Meanwhile, the signal carrying x_1 is aligned with the direction along which x_{02} is transmitted. Then, the receive filter being orthogonal to the above aligned direction is adopted so as to recover x_{01} and eliminate the branch damaged by x_1. x_{01} is transmitted via the principal sub-channel corresponding to the largest singular value $\lambda_{01}^{\mathrm{m}}$ of H_0^{m}. Since $P_0 = V_0^{\mathrm{m}}$ is employed, we let $H_1^{\mathrm{m}} p_1 = u_{02}^{\mathrm{m}}$ so as to achieve the alignment of x_1 to x_{02}. Then, $p_1 = (H_1^{\mathrm{m}})^{-1} u_{02}^{\mathrm{m}}$ is obtained. By applying normalisation to p_1, we have $p_1 \leftarrow p_1/\|p_1\|$. We choose U_0^{m} as the receive filter, then the estimated signal at MBS is given by

$$\bar{y}_{\mathrm{m}} = \begin{bmatrix} \sqrt{\dfrac{P_{\mathrm{m}}}{2}} \rho_{\mathrm{MU}}^{-\alpha/2} \lambda_{01}^{\mathrm{m}} x_{01} \\ \sqrt{\dfrac{P_{\mathrm{m}}}{2}} \rho_{\mathrm{MU}}^{-\alpha/2} \lambda_{02}^{\mathrm{m}} x_{02} + \dfrac{\sqrt{P_{\mathrm{p}}} \rho_{\mathrm{PU}}^{-\alpha/2}}{\|(H_1^{\mathrm{m}})^{-1} u_{02}^{\mathrm{m}}\|} x_1 \end{bmatrix} + (U_0^{\mathrm{m}})^{\mathrm{H}} n \tag{7}$$

We can see from (7) that x_{01} could be recovered without interference, whereas x_{02} is subjected to the interference from PU. The bandwidth normalised data rate for the transmission of x_{01} can be easily obtained as

$$R_{01} = \log_2\left\{1 + \frac{P_m \rho_{MU}^{-\alpha}(\lambda_{01}^m)^2}{2\sigma_n^2}\right\} \quad (8)$$

Under the assumption of inter-BS collaboration, MBS feeds decoded x_{01} to PBS via backhaul for interference cancellation in the latter. The received signal at PBS is expressed as

$$y_p = \sqrt{\frac{P_m}{2}} r_{MU}^{-\alpha/2} H_0^p p_{01} x_{01} + \sqrt{\frac{P_m}{2}} r_{MU}^{-\alpha/2} H_0^p p_{02} x_{02}$$
$$+ \sqrt{P_p} r_{PU}^{-\alpha/2} H_1^p p_1 x_1 + n \quad (9)$$

Based on H_0^p, the precoder p_{01} and data x_{01} obtained from MBS, the first term on the right-hand side (RHS) of (9) can be eliminated with interference cancellation. Substituting $p_{02} = v_{02}^m$ into (9), and adopting f_1 and f_2 to recover x_{02} and x_1 at PBS, respectively, we can obtain

$$\begin{cases} \bar{y}_p^{(02)} = \sqrt{\frac{P_m}{2}} r_{MU}^{-\alpha/2} f_1^H H_0^p v_{02}^m x_{02} + \sqrt{P_p} r_{PU}^{-\alpha/2} f_1^H H_1^p p_1 x_1 + f_1^H n \\ \bar{y}_p^{(1)} = \sqrt{\frac{P_m}{2}} r_{MU}^{-\alpha/2} f_2^H H_0^p v_{02}^m x_{02} + \sqrt{P_p} r_{PU}^{-\alpha/2} f_2^H H_1^p p_1 x_1 + f_2^H n \end{cases} \quad (10)$$

By employing f_1 and f_2, x_{02} and x_1 can be recovered where x_1 is the desired data for PBS and x_{02} is fed to MBS. The main idea in the above processing is that, since the interference from MU to PBS is strong, PBS treats it as a useful signal and decodes it for MBS. As a reward, PU obtains communication opportunity by aligning its transmission to the spatial direction of non-principal sub-channel from MU to MBS. In what follows, we elaborate the filter vector design and derive the criterion of reception mode selection.

Since the randomness of wireless channel, spatial features of two mutually interfering signals carrying x_{02} and x_1 determined by $H_0^p v_{02}^m$ and $H_1^p p_1$, respectively, will change dynamically. Two types of reception schemes including matched filtering (MF) and zero-forcing (ZF) can be adopted at PBS. As shown in Fig. 3, take the reception of x_{02} as an example. MF refers to the same direction of filter vector f_{02}^M and desired signal's direction $H_0^p v_{02}^m$, with which no expected signal power loss is resulted. However, interference cannot be cancelled, i.e. the projection of $H_1^p p_1$ corresponding to interfering data x_1 onto the direction determined by $H_0^p v_{02}^m$ is non-zero. As for ZF reception, the filter vector f_1^O

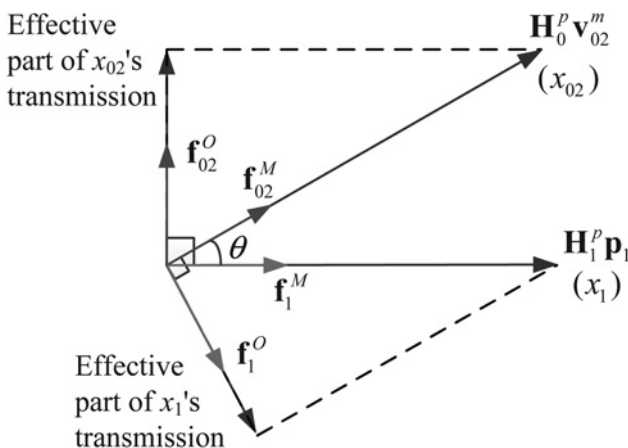orthogonal to the interference direction, $H_1^p p_1$ is adopted, so that interference is eliminated. However, desired signal power loss results. In practical use, flexible selection of the above two reception modes is dependent on both the relative strength of and spatial correlation between the mutually interfering signals.

For simplicity, we introduce two equivalent unit vectors $E_1 = H_0^p v_{02}^m / \|H_0^p v_{02}^m\|$ and $E_2 = H_1^p p_1 / \|H_1^p p_1\|$, which indicate the spatial feature of signals carrying x_{02} and x_1, respectively. Then, we can obtain MF vector $f_{02}^M = E_1$ and ZF vectors $f_{02}^O = (E_1 - E_2^H E_1 E_2)/\|E_1 - E_2^H E_1 E_2\|$. The achievable rates of x_{02} with different reception modes are computed as

$$R_{02}^M = \log_2\left\{1 + \frac{(P_m/2)r_{MU}^{-\alpha}\|(f_{02}^M)^H H_0^p v_{02}^m\|^2}{\sigma_n^2 + P_p r_{PU}^{-\alpha}\|(f_{02}^M)^H H_1^p p_1\|^2}\right\} \quad (11)$$

$$R_{02}^O = \log_2\left\{1 + \frac{P_m r_{MU}^{-\alpha}\|(f_{02}^O)^H H_0^p v_{02}^m\|^2}{2\sigma_n^2}\right\} \quad (12)$$

Similarly, R_1^M and R_1^O can be computed. Define the interference (carrying x_1) to the desired signal (carrying x_{02}) ratio as k

$$k = \frac{P_p r_{PU}^{-\alpha}\|H_1^p p_1\|^2}{(P_m/2)r_{MU}^{-\alpha}\|H_0^p v_{02}^m\|^2} = \frac{2P_p\|H_1^p p_1\|^2}{P_m\|H_0^p v_{02}^m\|^2}\left(\frac{r_{PU}}{r_{MU}}\right)^{-\alpha} \quad (13)$$

The spatial correlation of mutually interfering signals carrying x_{02} and x_1 can be evaluated by the square of cosine of the angle between the two signals

$$\cos^2\theta = \frac{E_1^H E_2 E_2^H E_1}{\|E_1\|^2\|E_2\|^2} = \|E_1^H E_2\|^2 \quad (14)$$

To derive the criterion for reception mode selection, we let $R_{02}^M = R_{02}^O$ and substitute (14) into (11) and (12), then we can obtain

$$k_{div} = \frac{1}{(P_m/2\sigma_n^2)r_{MU}^{-\alpha}\|H_0^p v_{02}^m\|^2(1 - \cos^2\theta)} \quad (15)$$

where $(P_m/2\sigma_n^2)r_{MU}^{-\alpha}\|H_0^p v_{02}^m\|^2$ denotes the desired signal (x_{02}) to noise ratio (SNR) observed at the receiver. In addition, $\cos^2\theta$ indicates the degree of spatial correlation of the two mutually interfering signals carrying x_{02} and x_1, respectively. Recall that k represents for the interference (x_1) to signal (x_{02}) ratio (ISR) as expressed by (13). Then, the criterion of reception mode selection
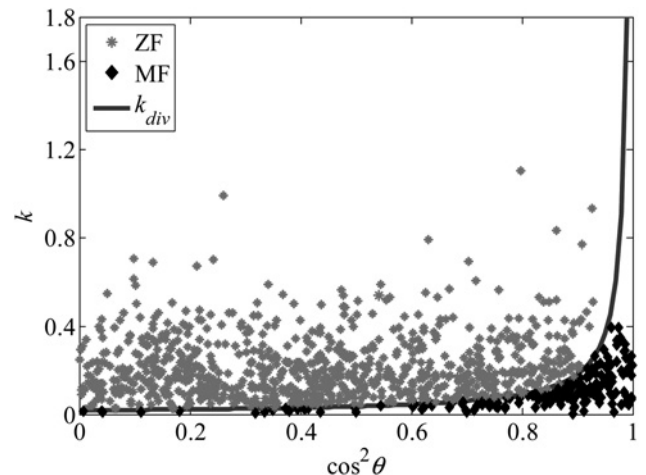

Fig. 3 Example of MF and ZF reception

Fig. 4 Adaptive reception mode selection

is given by (16) as

$$\begin{cases} \text{if } k \geq k_{\text{div}}, & \text{ZF is adopted} \\ \text{if } k < k_{\text{div}}, & \text{MF is adopted} \end{cases} \qquad (16)$$

where k_{div} is a dividing line derived from $R_{02}^{\text{M}} = R_{02}^{\text{O}}$. In practice, it can be obtained using some locally measurable information such as SNR, ISR, and the correlation index $\cos^2 \theta$ which can be calculated based on CSI and precoding information, in terms of (15). Then, current k which can be measured at PBS or computed following (13) is compared with k_{div}. Although we take the reception of x_{02} as an example, the reception of x_1 at PBS is similar, except for switching between signal and interference.

Let $r_{\text{MU}} = r_{\text{PU}} = d = 300$ m, $P_{\text{m}} = -10$ dBm, $\mu = 20$ and $\sigma_{\text{n}}^2 = -80$ dBm [4, 29]. Fig. 4 shows the optimal reception mode selection for x_{02} against $\cos^2 \theta$ and k under $\|H_0^{\text{p}} v_{02}^{\text{m}}\| = 0.995$. The dots are acquired by calculating R_{02}^{M} and R_{02}^{O} according to (11) and (12), and then choosing the larger one. Note that the grey asterisk and dark diamond are divided by k_{div}, i.e. the optimal reception mode selection can be achieved by (16). From (15), we can find that given specific $r_{\text{MU}}^{-\alpha}$, noise power σ_{n}^2 and spatial correlation between mutually interfering signals $\cos^2 \theta$, large P_{m} and/or a high spatial matching degree of precoding vector for expected transmission (v_{02}^{m}) and the interfering channel (H_0^{p}) would result in small k_{div}, i.e. the dark curve in Fig. 4 declines with increasing P_{m} and/or $\|H_0^{\text{p}} v_{02}^{\text{m}}\|$. In other words, the high strength of received desired signal and small $\cos^2 \theta$ will correspondingly yield high probability of choosing ZF as the optimal reception mode. MF is preferred only when the received expected signal is weak and $\cos^2 \theta$ is high. Moreover, it is worth noting that in the above discussion, PBS selects the reception mode based on SNR, ISR and $\cos^2 \theta$ which can be estimated by the receiver, making it easy for implementation.

The uplink rates of MU and PU are $R_{\text{m}} = R_{01} + \max(R_{02}^{\text{M}}, R_{02}^{\text{O}})$ and $R_{\text{p}} = \max(R_1^{\text{M}}, R_1^{\text{O}})$, respectively. $\max(\cdot)$ indicates selection of the maximum of candidate elements.

3.3 Signal processing in Z channel model

By leveraging interference locality, a Z channel model is obtained in which the cross-tier interferences are asymmetric as the one from PU to MBS is ignored. In this model, the received signal at MBS is

$$y_{\text{m}} = \sqrt{\frac{P_{\text{m}}}{2}} \rho_{\text{MU}}^{-\alpha/2} (H_0^{\text{m}} p_{01} x_{01} + H_0^{\text{m}} p_{02} x_{02}) + n \qquad (17)$$

Fig. 5 *Flowchart of ASCENT*

MU and MBS adopt signal processing suitable for spatial channel H_0^{m}, i.e. V_0^{m} and U_0^{m} are employed as transmit precoder and receive filters, respectively. Then, MBS decodes x_{01} and x_{02}, and shares them with PBS over backhaul.

The received signal at PBS is expressed by

$$y_{\text{p}} = \sqrt{\frac{P_{\text{m}}}{2}} r_{\text{MU}}^{-\alpha/2} H_0^{\text{p}} (p_{01} x_{01} + p_{02} x_{02}) + \sqrt{P_{\text{p}}} r_{\text{PU}}^{-\alpha/2} H_1^{\text{p}} p_1 x_1 + n \quad (18)$$

As the interference from PU to MBS is ignored, PU and PBS adopt transmission mode matching with H_1^{p}. Let $p_1 = v_{11}^{\text{p}}$. PU subtracts data vector $x_0 = [x_{01} \quad x_{02}]^{\text{T}}$ from y_{p}, (18) becomes

$$y_{\text{p}} = \sqrt{P_{\text{p}}} r_{\text{PU}}^{-\alpha/2} H_1^{\text{p}} v_{11}^{\text{p}} x_1 + n \qquad (19)$$

By employing $f_1 = u_{11}^{\text{p}}$ as receive filter, x_1 is readily obtained. On the basis of the above discussion, PBS implements interference cancellation via BS-side collaboration. In fact, in this case the uplink communications in both macrocell and picocell are equivalent to point-to-point MIMO. Bandwidth normalised rate for the transmission of x_1 is obtained as

$$R_1 = \log_2 \left\{ 1 + \frac{P_{\text{p}} r_{\text{PU}}^{-\alpha} (\lambda_{11}^{\text{p}})^2}{\sigma_{\text{n}}^2} \right\} \qquad (20)$$

Although the algorithms in this subsection are based on the asymmetrical cross-tier interference assumption, there exists interference in reality. As a result, the achievable rates of MU and PU should be calculated according to $R_{\text{m}} = R_{01} + R_{02}$ and $R_{\text{p}} = R_1$, as given by (5) and (20).

Based on the description in Section 3, the proposed ASCENT can be illustrated in Fig. 5.

4 Extension of ASCENT

So far, we focused on one-picocell system settings for simplicity. However, in practice, multiple picocells may overlay on top of a macrocell. Fortunately, ASCENT can be easily extended to this general case as we will discuss next. Suppose L picocells have been overlaid atop of a macrocell. As discussed in Section 2, we assume inter-picocell interference can be avoided via operator's management or orthogonal resource allocation. Each PBS independently executes ASCENT to decide which channel model and signal processing to use. As a result, different decisions may be made by L PBSs.

For those selecting X channel in an arbitrary time slot, each user is activated by the MBS and a PBS. Since MBS and PBSs can cooperate with each other via reliable backhaul and under the control of the same operator, the optimal assistant PBS, denoted by PBS$_{l^*}$ ($l^* \in \{1, \dots, L\}$), can be selected to produce the highest uplink transmission rate of x_{02} originally transmitted from MU to MBS. On the other hand, in each picocell, one user, say PU$_l$ ($l \in \{1, \dots, L\}$) is scheduled to send x_l to PBS$_l$ using BF. The precoder at PU$_l$ should meet the condition $H_l^{\text{m}} p_l = u_{02}^{\text{m}}$ to align x_l with x_{02}, where H_l^{m} is the channel matrix from PU$_l$ to MBS. Then, the second row on the RHS of (7) becomes $\sqrt{P_{\text{m}}/2} \rho_{\text{MU}}^{-\alpha/2} \lambda_{02}^{\text{m}} x_{02} + \sum_{l=1}^{L} (\sqrt{P_{\text{p}}} \rho_{\text{PU}_l}^{-\alpha/2} / \|(H_l^{\text{m}})^{-1} u_{02}^{\text{m}}\|) \psi_l x_l$. Here $\rho_{\text{PU}_l}^{-\alpha/2}$ indicates the distance from PU$_l$ to MBS. ψ_l is an indicator function. When $\psi_l = 1$, signal processing based on X channel mode is employed, otherwise Z channel is adopted. As a result, x_{01} can be recovered at MBS and shared with all the other PBSs, whereas x_{02}, subjected to the interference from L uplink transmissions, is decoded by PBS$_{l^*}$ and fed to MBS as well as the other PBSs. As for PU$_l$, its data x_l is recovered by the intended receiver PBS$_l$. For those adopting the Z channel model, each picocell independently implements signal processing given in Section 3.3.

Algorithm 1
Initialisation:
MU, PU_l, MBS and PBS_l acquire CSI; MU adopts $\mathbf{P}_0 = \mathbf{V}_0^m$ to transmit; MBS employs $\mathbf{F}_0 = \mathbf{U}_0^m$ to decode x_{01};
Procedure:
1:   PBS_l obtains x_{01} from MBS;
2:   PBS_l calculates η based on Eqs. (5) and (6);
3:   **if** $\eta \geq \eta_{th}$ **then**
4:     PU_l adopts $\mathbf{p}_l = \mathbf{v}_{l1}^p$ to transmit;
5:     PBS_l obtains x_{02} from PBS_{l^*}, subtracts x_{01} and x_{02} from its received signal and adopts $\mathbf{u}_{l1}^p$ to recover x_1;
6:   **else**
7:     PU_l adopts $\mathbf{p}_l = \frac{(\mathbf{H}_l^m)^{-1}\mathbf{u}_{02}^m}{\|(\mathbf{H}_l^m)^{-1}\mathbf{u}_{02}^m\|}$ to transmit;
8:     PBS_l subtracts x_{01} from received signal;
9:     **if** $l = l^*$ **then**
10:       PBS_l calculates k and k_{div} based on Eqs. (13), (14) and (15);
11:       **if** $k \geq k_{div}$ **then**
12:         PBS_l adopts ZF to recover x_{02};
13:       **else**
14:         PBS_l adopts MF to decode x_{02};
15:       **end if**
16:       PBS_l feeds x_{02} to MBS and other PBSs;
17:       PBS_l executes from step 10 to 15 with x_{02} being replaced by x_1;
18:     **else**
19:       PBS_l executes step 17;
20:     **end if**
21: **end if**

Fig. 6 *eASCENT*

However, we need to account for the differences of this extended ASCENT (eASCENT) from the original ASCENT. First, due to the different decisions made by L picocells, the delivery of x_{01} will be disturbed by multiple PUs adopting signal processing based on the Z channel. The aggregate interference is $\sum_{l=1}^{L}(1 - \psi_l)\sqrt{P_p}\rho_{PU_l}^{-\alpha/2}(\boldsymbol{u}_0^m)^H \boldsymbol{H}_l^m \boldsymbol{p}_l x_l$. Although each PU transmits under the constraint $\eta \geq \eta_{th}$, the accumulated influence to the MU's uplink transmission may be significant. Therefore, the total interference constraint, η_{th}^{tot} may be used in conjunction with η_{th} to guarantee the MU's data transmission. η^{tot} can be derived from (5) and (6). Due to space limitation, the details are omitted. Second, the transmission of x_{02} will be disrupted as long as one picocell employs the X channel. In this case, x_{02} cannot be decoded by MBS and, instead, is shared by the assistant PBS_{l^*} with the MBS and other PBSs.

Algorithm 1 (see Fig. 6) describes the eASCENT reflecting the above description. Each PU_l-PBS_l pair executes this algorithm independently. For simplicity, we assume that at least one picocell adopts the X channel while the others employ the Z channel model. Moreover, the assistant PBS_{l^*} has been selected by MBS. If only one picocell is deployed within the coverage of the macrocell, or all picocells choose the same interference model, the original ASCENT can be directly applied. In summary, for L picocells overlaid atop of a macrocell, the eASCENT can simultaneously support $L + 2$ data streams: 2 from MU to MBS and L transmissions between L PU-PBS pairs. It should be noticed that the above result is under $N_r^p = N_r^m = N_t^p = N_t^m = 2$ system settings. That is, there is no requirement of additional antennas at
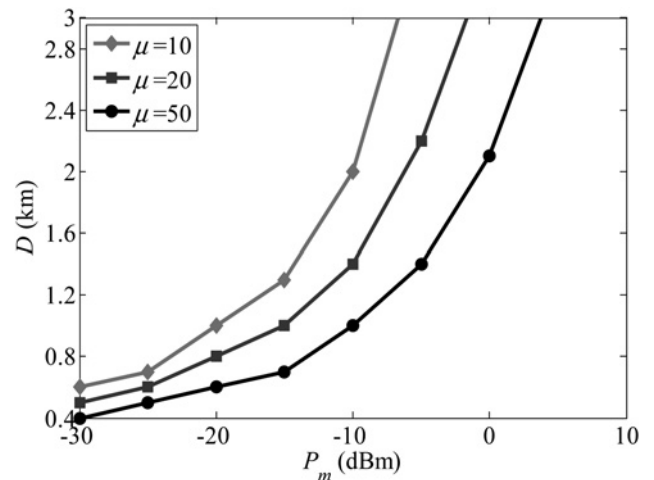
either MBS or PBS when L increases. This is because MBS only cares about its desired data stream(s), i.e. interference status is transparent to the macro transmission, whereas for the PBS, it has sufficient DoFs to distinguish its intended signal from the single interference from MU (the other one is eliminated at PBS by employing IC).
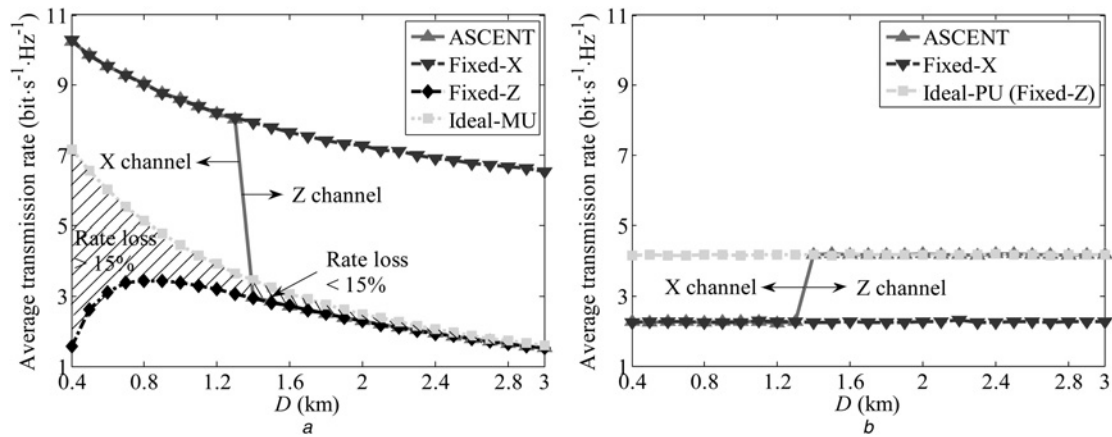
5 Simulation results

We now evaluate the performance of ASCENT via MATLAB simulation. For simplicity, we assume multiple picocells with the same features, and inter-picocell interference is negligible, as described in Section 2. As a result, the total uplink throughput w.r.t. picocell systems will linearly increase with the number of picocells. As for the transmission of x_{02}, a multi-PBS diversity gain can be obtained. For conciseness, the simulation is based on one-picocell system settings as shown in Fig. 1, but results for multiple picocells can be easily derived. Parameters used in the simulation are given in Table 1 [4, 26–29].

Table 1 Simulation parameters

Parameter	Value
P_m	[–30, 15] dBm
P_p	P_m/μ
μ	{10, 20, 50}
α	2
σ_n^2	–80 dBm
r_{MU}, r_{PU}, d	300 m
D	[0.4, 3] km
α_{PU}	π
$\alpha_{MU}, \theta_{MU}, \theta_{PU}$	0
η_{th}	0.85

Fig. 7 *X channel and Z channel regions*

Fig. 8 *Comparison of average transmission rate*
a MU's rate
b PU's rate

Fig. 7 demonstrates the division of symmetric (X channel) and asymmetric (Z channel) interference regions based on the distance from MBS to PBS (D) and transmit power (P_m and P_p). We set $\eta_{th} = 0.85$, i.e. rate degradation caused by neglecting cross-tier interference from PU to MBS should be less than 15%. The line with square marker ($\mu = 20$) in Fig. 7 is obtained by projecting points in Fig. 2*b* whose $\eta = 0.85$, onto the $D - P_m$ plane. For the points determined by D and P_m locating in the left and upper regions of the curve, interference from PU to MBS could be ignored. Otherwise, such cross-tier interference should be taken into account. To illustrate how the dividing line changes with μ, other two lines under $\mu = 10$ and $\mu = 50$ are also plotted. As μ increases, the dividing line declines, which is consistent with what is shown in Fig. 2*a*.

Fig. 8 plots the average transmission rate of ASCENT in comparison with other two strategies, including X channel (fixed-X) and Z channel (fixed-Z) based transmission, respectively, under $P_m = -10$ dBm and $\mu = 20$. With fixed-X, the relationship between the desired signal and interference is exploited to implement adaptive reception mode selection (see in Section 3.2). Both MU's and PU's rate are simulated. Note that the unit of y-axis is bit $\cdot$ s^{-1} $\cdot$ Hz^{-1}, i.e. the rate is normalised by transmission bandwidth. To illustrate the effect of BS-side collaboration on the uplink communication of both MU and PU, transmission rates of MU and PU without inter-BS cooperation are also plotted, called ideal-MU and ideal-PU, respectively. Note that in these cases, when MU transmits, PU keeps silent so that no interference is introduced to MBS, and vice versa.

For the transmission of MU as shown in Fig. 8*a*, when D is small, $\eta < \eta_{th}$, so interference from PU should be considered. The signal processing in X channel model is employed. ASCENT and fixed-X output the same R_m. Since x_{02} is decoded by PBS, which is closer to MU than MBS, and then fed to MBS through backhaul. With the help of PBS, MU's uplink performance is significantly improved compared with that with Ideal-MU. As D grows gradually, the gap of R_m with fixed-Z and ideal-MU narrows, due to the fact that the strength of interference from PU to MBS ignored by using fixed-Z reduces with increasing D, and as a result, the rate degradation diminishes. When $D > 1.4$ km, the performance loss of MU due to ignoring of cross-tier interference is less than 15%, i.e. the ratio of fixed-Z to ideal-MU exceeds 0.85. Then signal processing based on Z channel is employed. ASCENT and fixed-Z output the same R_m. As D increases further, R_m obtained by ASCENT approaches that with ideal-MU. With fixed-Z, MU's rate improves first with increasing D when D is small, since cross-tier interference which is the dominant factor affecting MU's rate, reduces as D grows. When $D > 0.8$ km, although increasing D can still reduce cross-tier interference, desire signal transmission of MU is also deteriorated, eventually surpassing the performance improvement brought by cross-tier

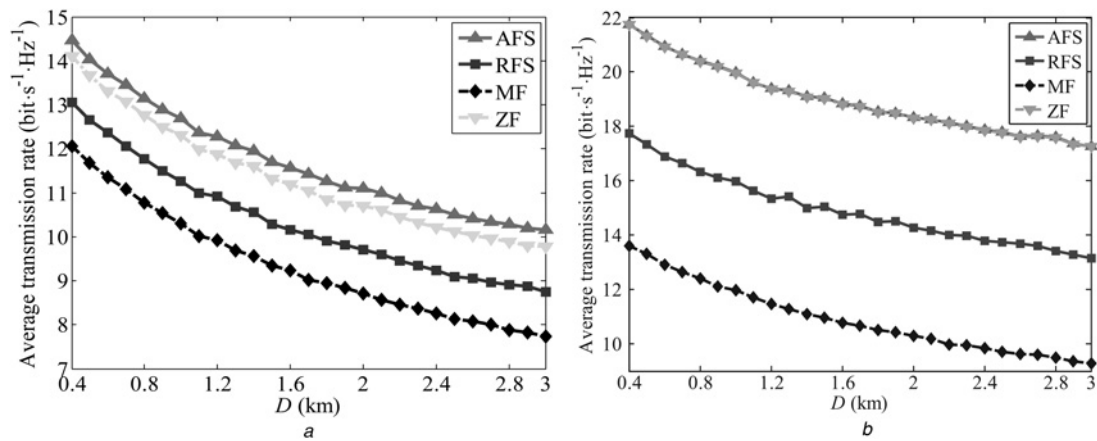interference reduction. So that MU's rate decreases as D grows too large.

For the transmission of PU as shown in Fig. 8*b*, when D is small, ASCENT is equivalent to fixed-X, signal processing at both PU and PBS should be designed in accordance with MU's uplink transmission, thus resulting in poor rate performance of PU. As D increases and $\eta \geq \eta_{th}$ holds, Z channel model is used, in which PU and PBS adopt transmit precoder and receive filter matching their own channel, and thus R_p is improved over that with fixed-X. Since R_p of ideal-PU is dependent on d rather than D, it remains constant. As for fixed-Z, transmission from PU to PBS is based on their own channel condition. Moreover, interference from MU can be eliminated at PBS by employing IC. As a result, the achievable rate of PU, R_p, with fixed-Z is the same as that of ideal-PU, indicated by the light grey horizontal line in Fig. 8*b*.

In summary, when D is small, PBS helps MU by decoding its information and sharing it with MBS, thus improving R_m significantly. However, there is a performance loss of R_p. As D grows large, interference from PU to MBS can be ignored, so PU transmits to PBS for its own benefit and no longer yields to the MU's transmission. As a result, R_p is improved while guaranteeing R_m. As can be seen from the figures, a step change of MU's and PU's rate appears near $D = 1.4$ km (i.e. trip point) due to the adaptation between the two interference models. By properly selecting η_{th}, the above trip point can move along the x-axis. From the theoretical analysis in the previous sections and the simulation results given in Fig. 8, we can see that the processing under the X channel model is much more complicated than that in the Z channel model. Moreover, MU's rate is significantly enhanced with the X channel based processing, whereas the PU's rate is lossless by adopting the Z channel based processing. ASCENT can guarantee the rate performance of and achieve the fairness among MU and PU by intellectually selecting appropriate interference model in accordance with the changing communication environment.

In Fig. 9, the achievable system sum-rate normalised by transmission bandwidth, i.e. $R_m + R_p$ adopting MF, ZF, adaptive filter selection (AFS) and random selection of the above two types of filters (Random filter selection (RFS)) are evaluated. Simulation is carried out with $P_m = 0$ dBm and $\mu = 20$, since in this case, interference from PU to MBS cannot be ignored for any D within the range [0.4, 3] km, then adaptive reception is meaningful in the X channel model. Moreover, these two subfigures are plotted under $\cos^2 \theta > 0.95$ and arbitrary $\cos^2 \theta$, respectively.

When mutually interfering signals are highly correlated, AFS outputs an obvious rate improvement compared to the other methods. However, when $\cos^2 \theta$ is totally random, the performance of AFS is almost the same as that with ZF. This is because given $P_m = 0$ dBm and $\mu = 20$, cross-tier interference is the dominant factor affecting each user's uplink transmission rate.

Fig. 9 *Comparison of system sum-rate with different reception schemes*
a $\cos^2\theta > 0.95$
b Arbitrary $\cos^2\theta$

Thus, eliminating interference is preferred rather than maintaining the expected signal's power with non-zero residual interference. From Fig. 9, one can also see that the rate performance under high signal-interference correlation is severely degraded compared with that under general $\cos^2\theta$ values. This is due to the fact that when the interference signal is highly correlated with the desired signal, severe CCI results, which will either cause serious signal deterioration with ZF or large residual interference power with MF.

6 Conclusion

In this paper, an adaptive mechanism exploiting interference locality and relationship between desired signal and interference (ASCENT) is proposed for uplink transmission in HetNet. In the strategy design, inter-BS collaboration is exploited, and practical factors including path loss, relative locations of multiple cells, and power difference between nodes are taken into account. Two types of interference models were investigated. In the X channel, PBS uses information shared by MBS to cancel local interference, and decodes the data carried by strong interference from MU, which is then fed to MBS, and in exchange, PU obtains communication opportunity by aligning its transmission with one of the sub-channels from MU to MBS. In addition, adaptive reception based on spatial correlation and strength of desired signal and interference is adopted at PBS, with which a good tradeoff between interference suppression and the desired level of signal distortion can be achieved. For the Z channel, since the cross-tier interference from PU to MBS is ignored, PU and PBS adopt precoding and filtering processing suitable for their own channel condition, so PU's uplink rate is improved while the performance of MU is guaranteed. In addition, ASCENT can be easily extended to the general case where multiple picocells are involved. In summary, the proposed mechanism can accommodate multiple concurrent uplink transmissions from MU and PU. By effectively exploiting interference locality and signal-interference interrelation, both MU's and PU's performance can be adaptively improved.

ASCENT is applicable to multiple picocells overlaid on top of a macrocell. However, we assumed in this paper that the MBS is equipped with only two antennas to serve one MU, and inter-picocell interference is negligible. When $N_r^m > 2$, multiple MUs can be supported simultaneously, but their interferences to uplink transmission in each picocell will become more complicated. In this case, we could assign each MU to a proper, e.g. its adjacent picocell so that the MU can be cooperatively served by its designated PBS. Then, via inter-BS information sharing, interference from multiple MUs could be mitigated at the PBSs. Moreover, if inter-picocell interference cannot be avoided due to the high density of picocell. Cooperation among PBSs as well as between PBSs and MBS such as joint processing and information exchanging should be effectively exploited to handle these interferences. How to select the assistant PBS for each MU to achieve high throughput is also an important issue to be addressed. These are matters of our future inquiry.

7 Acknowledgments

8 References

1 Sundaresan, K., Arslan, M.Y., Singh, S., *et al.*: 'FluidNet: A flexible cloud-based radio access network for small cells'. Proc. the ACM Int. Conf. Mobile Computing & Networking (Mobicom), Miami, USA, October 2013, pp. 99–110
2 Nakamura, T., Nagata, S., Benjebbour, A., *et al.*: 'Trends in small cell enhancements in LTE advanced', *IEEE Commun. Mag.*, 2013, **51**, (2), pp. 98–105
3 Damnjanovic, A., Monyojo, J., Wei, Y., *et al.*: 'A survey on 3GPP heterogeneous networks', *IEEE Wirel. Commun.*, 2011, **18**, (3), pp. 10–21
4 Quek, T.Q.S., Roche, G., Kountouris, M.: 'Small cell networks: deployment, PHY techniques, and resource management' (Cambridge University Press, 2013)
5 Arslan, M.Y., Yoon, J., Sundaresan, K., *et al.*: 'FERMI: A femtocell resource management system for interference mitigation in OFDMA networks'. Proc. the ACM Int. Conf. Mobile Computing & Networking (Mobicom), Las Vegas, USA, September 2011, pp. 25–36
6 Mukherjee, A., De, D., Deb, P.: 'Interference management in macro-femtocell and micro-femtocell cluster-based long-term evaluation-advanced green mobile network', *IET Commun.*, 2016, **10**, (5), pp. 468–478
7 Yoon, J., Sundaresan, K., Khojastepour, M.A., *et al.*: 'ProBeam: a practical multicell beamforming system for OFDMA small-cell networks'. Proc. the ACM Int. Symp. Mobile Ad Hoc Networking and Computing (MobiHoc), Bangalore, India, August 2013, pp. 147–156
8 Qian, M., Hardjawana, W., Li, Y., *et al.*: 'Inter-cell interference coordination through adaptive soft frequency reuse in LTE networks'. Proc. the IEEE Wireless Communications and Networking Conf. (WCNC), Paris, France, April 2012, pp. 1618–1623
9 Kamel, M.I., Elsayed, K.M.F.: 'Performance evaluation of a coordinated time-domain eICIC framework based on ABSF in heterogeneous LTE-Advanced networks'. Proc. the Global Communications Conf. (GLOBECOM), Anaheim, USA, December 2012, pp. 5326–5331
10 Ayach, O.E., Peters, S.W., Heath, R.W.: 'The practical challenges of interference alignment', *IEEE Wirel. Commun. Mag.*, 2013, **20**, (1), pp. 35–42
11 Lee, H., Ko, Y.: 'Linear transceiver design based on interference alignment for MIMO heterogeneous networks'. Proc. the IEEE Int. Symp. Personal Indoor and Mobile Radio Communications (PIMRC), Sydney, Australia, September 2012, pp. 1645–1650
12 Shin, W., Noh, W., Jang, K., *et al.*: 'Hierarchical interference alignment for downlink heterogeneous networks', *IEEE Trans. Wirel. Commun.*, 2012, **11**, (12), pp. 4549–4559
13 Yetis, C.M., Gou, T., Jafar, S.A., *et al.*: 'On feasibility of interference alignment in MIMO interference networks', *IEEE Trans. Signal Process.*, 2010, **58**, (9), pp. 4771–4782
14 Razaviyayn, M., Lyubeznik, G., Luo, Z.Q.: 'On the degrees of freedom achievable through interference alignment in a MIMO interference channel', *IEEE Trans. Signal Process.*, 2012, **60**, (2), pp. 812–821

15 Razavi, M.S., Ratnarajah, T.: 'Interference alignment in k-user multiple-input-multiple-output interference channels with partially coordinated receivers', *IET Commun.*, 2014, **8**, (1), pp. 50–57

16 Li, L.E., Alimi, R., Shen, D., *et al.*: 'A general algorithm for interference alignment and cancellation in wireless networks'. Proc. the IEEE Int. Conf. Computer Communications (INFOCOM), San Diego, USA, March 2010, pp. 1–9

17 Li, Z., Cui, S., Shin, K.G.: 'Coordinated multi-point transmissions based on interference alignment and neutralization'. Proc. the IEEE Int. Conf. Computer Communications (INFOCOM), San Francisco, USA, April 2016, pp. 658–666

18 Zhang, X., Khojastepour, M.A., Sundaresan, K., *et al.*: 'Exploiting interference locality in coordinated multi-point transmission systems'. Proc. the IEEE Int. Conf. Communications (ICC), Ottawa, Canada, June 2012, pp. 4207–4211

19 Guillaud, M., Gesbert, D.: 'Interference alignment in partially connected interfering multiple-access and broadcast channels'. Proc. the Global Telecommunications Conf. (GLOBECOM), Houston, USA, December 2011, pp. 5–9

20 Qu, X., Kang, C.G.: 'A closed-form solution to implement interference alignment and cancellation for a Gaussian interference multiple access channel', *IEEE Trans. Wirel. Commun.*, 2014, **13**, (2), pp. 710–723

21 Liu, G., Sheng, M., Wang, X., *et al.*: 'Interference alignment for partially connected downlink MIMO heterogeneous networks', *IEEE Trans. Commun.*, 2015, **63**, (2), pp. 551–564

22 Ruan, L., Lau, V.K.N.: 'Dynamic interference mitigation for generalized partially connected quasi-static MIMO interference channel', *IEEE Trans. Signal Process.*, 2011, **59**, (8), pp. 3788–3798

23 Ruan, L., Lau, V.K.N., Rao, X.: 'Interference alignment for partially connected MIMO cellular networks', *IEEE Trans. Signal Process.*, 2012, **60**, (7), pp. 3692–3701

24 Wang, R., Du, Y.: 'Het-net throughput analysis with picocell interference cancellation'. Proc. the IEEE Int. Conf. Communications Workshops (ICC), Kyoto, Japan, June 2011, pp. 1–6

25 Maddah-Ali, M.A., Motahari, A.S., Khandani, A.K., *et al.*: 'Communication over MIMO X channels: Interference alignment, decomposition, and performance analysis', *IEEE Trans. Inf. Theory*, 2008, **54**, (8), pp. 3457–3470

26 Rappaport, T.S.: 'Wireless communications principles and practice' (Prentice-Hall, 2002, 2nd edn. 2002)

27 3GPP TR36.931: 'Evolved universal terrestrial radio access (E-UTRA); radio frequency (RF) requirements for LTE pico node B', 2014

28 Agrawal, A.: 'Heterogeneous networks: A new paradigm for increasing cellular capacity', http://netseminar.stanford.edu/seminars/01-29-09.pdf, accessed 23 June 2015

29 3GPP TS36.101: 'Evolved universal terrestrial radio access (E-UTRA); user equipment (UE) radio transmission and reception', 2013